Analyst

PAPER

View Article Online
View Journal

Cite this: DOI: 10.1039/c9an01779h

Oxidization increases the binding of EGCG to serum albumin revealed by kinetic data from label-free optical biosensor with reference channel†

Beatrix Peter, *‡ Andras Saftics, ‡ Boglarka Kovacs, ‡ Sandor Kurunczi and Robert Horvath

Received 10th September 2019,
Accepted 14th November 2019

DOI: 10.1039/c9an01779h

rsc.li/analyst

Epigallocatechin-gallate (EGCG) is the main polyphenol ingredient of green tea. This compound is a strong antioxidant and oxidizes easily. Numerous studies demonstrated its beneficial effects on the human health, for example its anticancer and anti-inflammatory activity. In the body, EGCG is transported by serum albumin. EGCG easily oxidizes and the interactions of the oxidized form presumably present significant differences. However, the presence of oxidized EGCG is usually neglected in the literature and its effects have not been investigated in detail. Here, we applied the label-free grating coupled interferometry method that performs dual-channel measurements. The measured kinetic signal can be compensated with a signal of a reference channel at each measurement time. By testing both hydrophilic and hydrophobic platforms, we found that EGCG can bind to a wide range of surfaces. Exploiting the dual-channel referencing ability as well as the unique sensitivity and throughput of the employed label-free technique, the experiments revealed the specific interactions between bovine serum albumin (BSA) and EGCG and determined the characteristic dissociation constant (K_d) of the binding equilibrium. The obtained binding constants were compared to literature values, showing reasonable agreement with NMR data. Besides the native EGCG, the oxidized form of EGCG was also examined, whose binding behaviors to serum albumins have never been studied. Overstoichiometric binding obtained; BSA has stronger and weaker binding sites, which could be characterized by two separate K_d values. Furthermore, EGCG oxidization increased the bound amount.

Introduction

Green tea infusion is from the unfermented leaves of *Camellia sinensis*. The main ingredient of this popular drink is the most studied polyphenol, epigallocatechin-gallate (EGCG). Numerous studies have demonstrated its beneficial effects on human health. For example its anti-cancer, anti-inflammatory, anti-cardiovascular, anti-metastasis and antioxidant activity have been established in many publications.[1–3] It is well known that tea polyphenols have antioxidant activities.[1,4] Among these ingredients, EGCG is the most effective in reacting with ROS (reactive oxygen species).[1,5] It has been demonstrated that EGCG and other catechin compounds are unstable at pH above 7 (neutral and alkaline conditions) and at high temperature, furthermore, it has been also shown that EGCG dimerizes and oxidizes facilely.[1,4,6] The color of the aqueous EGCG solution alters from colorless at around pH 7 to yellow at higher pH regions.[1,6] Its major oxidation products are theasinensin A (molecular weight 914 Da) and another dimer with molecular weight of 884 Da.[1,4,7] These dimers can be further transformed to other chemicals, supposedly polymers.[1,7]

In the body, EGCG is transported by serum albumin.[8] According to some studies, it has been suggested that the binding to plasma proteins – BSA (bovine serum albumin) and/or HSA (human serum albumin) – stabilizes EGCG, inhibits its oxidation *in vivo*, and masks its reactivity during transport through the bloodstream.[8–10] Thus, the cells can be protected from EGCG-induced cell death, and may allow effective delivery of the intact bioactive compound to target tissues without collateral damage.[8–10] EGCG can bind to certain cellular proteins as well, such as caspase-3, poly (ADP-ribose) polymerase (PARP), α-tubulin, Bcl2 proteins, vimentin, insulin-like growth factor receptor 1 (IGF1R), tyrosine-protein kinase fyn (FYN), glycine-rich RNA-binding protein 8 (GRP8), zeta-chain-associated protein kinase 70 (ZAP70), Ras-GTPase-activating protein-binding protein 1 (G3BP1), peptidyl-prolyl *cis*/*trans* isomerase (Pin1), signal transducer and activator of transcription 1 (STAT1), and 67 kDa laminin receptor (67LR).[10,11] In some cases, the binding has important biological consequences and

Nanobiosensorics Group, Centre for Energy Research, Institute of Technical Physics and Materials Science, Konkoly-Thege Miklós út 29-33, H-1121 Budapest, Hungary. E-mail: pbeatrix@mfa.kfki.hu

†Electronic supplementary information (ESI) available. See DOI: 10.1039/c9an01779h

‡Contributed equally to this work.

activates signaling pathways. For example, EGCG increased the viscosity of salivary mucin[1,12] and caused gelation and precipitation as well.[1,13] Recent studies showed that this compound inhibits protein aggregation and efficiently blocks the amyloid-fibril formation of amyloidogenic proteins (huntingtin, α-synuclein and amyloid-β) involved in Huntington's, Parkinson's and Alzheimer's diseases.[1,14,15] Furthermore, experiments on animal models suggest that drinking tea may decrease the incidence of dementia.[1,15] Additionally, it has neuroprotective and neurorescue activities in cellular and animal models of neurological disorders.[1,15] The biological activities of EGCG are mediated through the binding to the cell surface receptor 67LR.[1,16] The obstructive effect of the compound on tumor cell proliferation is exerted through its binding to 67LR and altering signaling pathways.[1,17]

In case of BSA, *in silico* docking analysis showed that BSA had stronger affinity to EGCG than other proteins.[10] Furthermore, the green tea polyphenol induces a conformational change in the protein BSA.[8]

The binding between BSA and EGCG was investigated previously mainly by labelling techniques, for example propidium iodide (PI) exclusion test, immunofluorescent staining, fluorescent quenching, western blot or other methods, such as nuclear magnetic resonance (NMR), circular dichroism (CD), size exclusion chromatography (SEC)[8,10,18–21] *etc*. A label-free technique, the quartz crystal microbalance with dissipation monitoring (QCM-D) was also applied to reveal the adsorbed mass, thickness and viscoelastic properties of EGCG adlayer on BSA surface at different EGCG concentrations, sodium chloride concentrations, temperatures and pH values.[22] It was suggested previously that EGCG binds to BSA both by hydrogen bonds and hydrophobic interactions and forms complexes.[8,10,18,20] According to a former study with QCM-D,[22] the adsorption isotherm of EGCG on BSA layer could be better described by the Freundlich model than the Langmuir model, showing that EGCG adsorption on BSA is dominated by nonspecific hydrophobic interactions.[22] Furthermore, EGCG adsorption reveals that hydrogen bonding might be also involved in EGCG adsorption on BSA surfaces.[22] The driving force of hydrophobic interaction may be attributed to the respective nonpolar structure of the polyphenol.[22] The hydroxyl groups of EGCG may form hydrogen bonds with H-acceptor sites on BSA, due to their proton-donating potential.[22,23] Change of pH and salt concentration can also influence the adsorption process, and the adsorbed EGCG molecules may act as bridges to let BSA molecules aggregate with each other.[22,24,25] However, water coupled to BSA are driven out during polyphenol adsorption.[22,24,25] Higher adsorbed mass of EGCG on BSA causes an increase in both viscosity and shear elastic modulus of the polyphenol adlayer.[22]

However, all of these investigations neglected the oxidized form of EGCG, except Kusuda and co-workers, who revealed that the oxidation of EGCG contributed to the formation of more stable complexes of EGCG and BSA.[20] Our previous work showed that EGCG and oxidized EGCG (hereafter ox. EGCG) form multilayers on poly(L-lysine)-*graft*-poly(ethylene glycol) (PLL-*g*-PEG) and its Arg-Gly-Asp (RGD) functionalized form (PLL-*g*-PEG-RGD).[26]

EGCG has been already studied by applying different optical label-free biosensors. Optical biosensors are especially suitable where label-free high-resolution kinetic data are needed for the analysis of surface adsorption processes.[27,28] The demonstrated high sensitivities enable the analysis of small molecules.[29–33] For example, the adsorption process and the subsequent HeLa cell adhesion onto PLL-*g*-PEG and PLL-*g*-PEG-RGD coatings were monitored by applying a multicomponent system with the label-free Epic BT resonant waveguide grating biosensor.[26] This publication highlighted the fact that in general, the significance of the oxidized form is neglected in other previous studies[26] and the description of the EGCG sample preparation is also deficient (freshly created or not, storage conditions, *etc*.) in former literature. Later, it was demonstrated that the temporal evolution of the adhesion process was largely affected by pre-exposing the HeLa cells to various concentrations of EGCG.[34,35] Using the Epic BT technique, the shape of the cell adhesion kinetic curves were employed to quantify *in vitro* cell viability in a fast, cost-effective, and highly sensitive manner.[34,35] The adsorption properties of EGCG-mucin complexes[36,37] as well as EGCG binding to PLL-*g*-PEG and PLL-*g*-PEG-RGD polymer coated surfaces[26] were studied by applying optical waveguide lightmode spectroscopy (OWLS).

In this study, another label-free technique, the grating coupled interferometry (GCI)[38–42] was chosen, to reveal the interactions of both EGCG and the rarely investigated ox. EGCG with BSA. In general, interferometric biosensors have several advantages including high sensitivity and ease of integration.[39,43–46] The present instrument has a leading level of sensitivity superior to surface plasmon resonance (reliable kinetics below 1 pg mm^{-2}, according to the manufacturer[47]). The capabilities of the device can be exploited in the drug discovery industry, especially in weak binding small molecule drugs, large drug targets, binding analysis at low concentrations and slow dissociation kinetics, among others.[47] Thus, it is especially suited to study small molecule interactions in a real-time and label-free manner. The further advantages compared to other ones are the robust microfluidics and crude sample robustness normally only achieved with plate-based assays.[47]

Our current work aimed to explore non-binding reference surface chemistries for EGCG analysis. EGCG and ox. EGCG can easily bind to proteins with high affinities through hydrogen bonding.[11,26] As demonstrated in our previous work, EGCG and ox. EGCG adsorbed even onto the strongly antifouling PLL-*g*-PEG coating as well.[26] Therefore, in the present work, we planned to reveal the binding of EGCG to BSA on hydrophilic and hydrophobic surfaces using the GCI technique. Another scope of this study was to understand the binding kinetics of EGCG. The employed high-throughput GCI setup Creoptix WAVE applies dual-channel measurements where the measured signal can be compensated with a reference channel signal at each measurement point. Exploiting this feature, our measurements allowed for the quantification of the specific binding and the dissociation constant (K_d) value of the BSA and EGCG/ox. EGCG interaction.

Materials and experimental methods

Materials

The buffer which was continuously flowed over the sensor surface (so-called running buffer) was prepared by adding 20 mM 4-(2-hydroxyethyl)-1-piperazine ethanesulfonic acid (HEPES, Sigma-Aldrich) to Hank's balanced salt solution (HBSS, Sigma-Aldrich). The pH was adjusted to pH 7.0 with 1 mM NaOH. 3% dimethyl sulfoxide (DMSO) was also added to the solution.

EGCG powder (Sigma Aldrich) was dissolved in running buffer in different concentrations. To get ox. EGCG solution, the liquid was placed into water bath for 90 min at 60–70 °C.[26]

Lyophilized BSA (Sigma Aldrich) was dissolved in running buffer to get BSA solution at 1 mg ml^{-1} concentration.

Grating coupled interferometry (GCI) measurements

Working principle of GCI. In a typical GCI device two light beams are coupled into a planar optical waveguide through two grating regions. The first beam, coupled into the waveguide through the first grating, passes through the sensing region of the waveguide. The beam, and thus also the coupled mode, is phase modulated using a square wave voltage driven liquid crystal modulator (LCM). The second beam is coupled in through the second grating, which also combines the two modes excited by the parallel beams (joins the two arms of the interferometer). Consequently, a periodic interference intensity signal is detected by a suitable photodetector and analyzed further. During the experiments, biomolecules adsorbing on the surface of the waveguide within the sensing region affect the phase of the propagating mode. This phase shift is precisely determined by analyzing the periodic interference signal.[38–42] To demonstrate the capabilities of this method, evaluated kinetic data were added to the ESI† about the binding of furosemide to carbonic anhydrase (CAII) protein, which is a widely employed reference system of kinetic measurements.

Chip conditioning and coating. The experiments and *in situ* monitoring of the binding events were performed using the

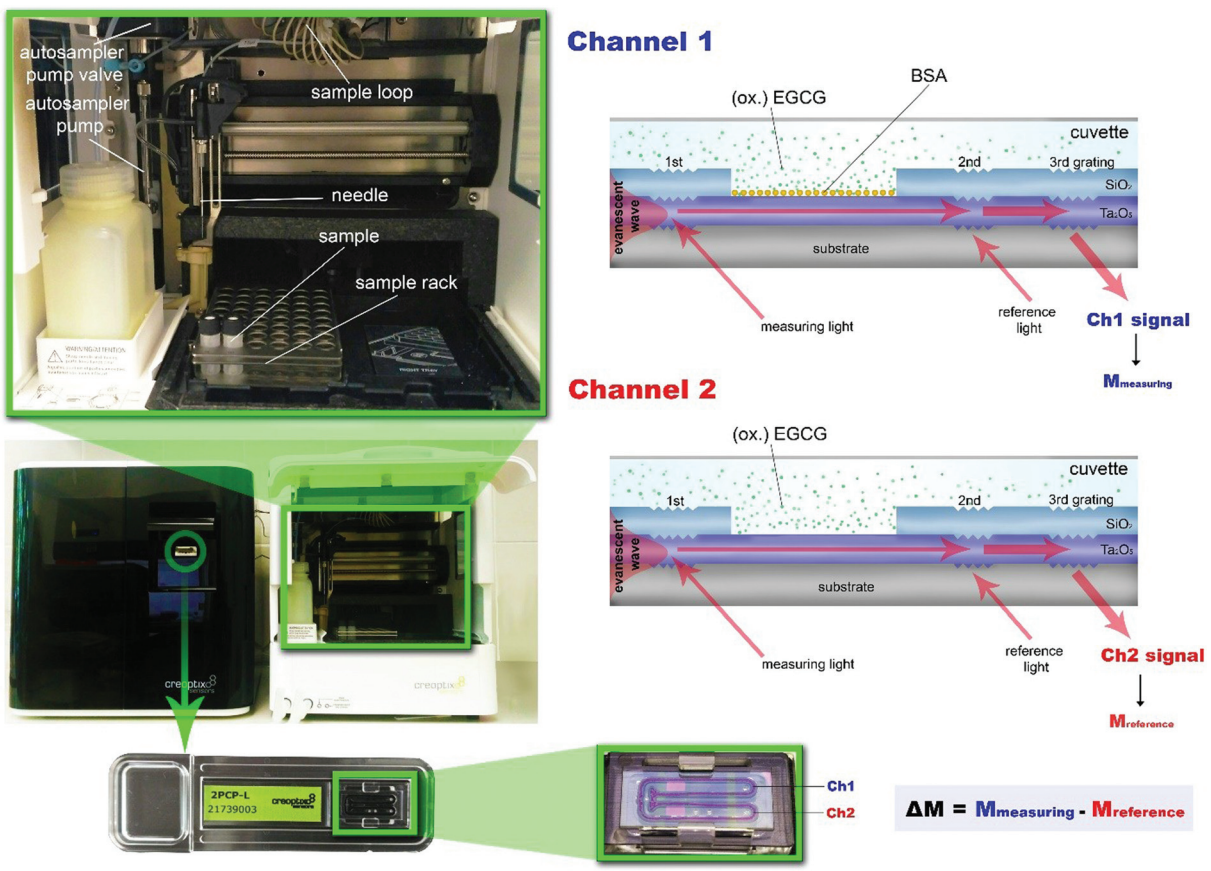

Fig. 1 The GCI instrument is on the left side (middle). The interior part of the appliance is magnified with a green frame. Here, the components (autosampler pump valve, autosampler pump, needle, sample rack) of the autosampler system and their layout is clearly seen (left side, above). The instrument applies a sensor chip (WAVEchip, bottom left corner). The sensor chips used in the WAVE instrument have two channels (bottom right corner); one for measuring the interaction between the immobilized bioreceptor and the analyte (measuring channel, *channel 1*) and one for subtracting the channel 1 signal by a reference signal (reference channel, *channel 2*). In our case, BSA was immobilized on *channel 1* surface, while *channel 2* remained unmodified.

Creoptix WAVE (Creoptix AG, Switzerland) GCI instrument.[38–42] The instrument has a temperature-controlled autosampler system (see Fig. 1) which enables to measure a number of samples in one experiment. Different types of WAVEchips (obtained from Creoptix AG, Switzerland) were used in the measurements, such as PCP (thin polycarboxylate functionalization, quasi-planar surface, hydrophilic), PCP-L (quasi-planar polycarboxylate coating with lipid anchors, hydrophobic) as well as Ta_2O_5. Based on our preliminary experiments performed on the above surfaces, PCP chips were chosen for the profound analysis of EGCG–BSA interaction.

We have to emphasize that it is difficult to find a reference surface or other protein which does not bind EGCG. According to our results, EGCG binds practically to any surfaces, it adsorbs to oxide type native chip surfaces (bare Ta_2O_5 chip surface) and it also coats hydrophobic surfaces (PCP-L chip surface, see ESI†). BSA has several sites which can form hydrogen bonds with water and potentially bind EGCG. More the surface is anti-fouling (water-like) it binds more EGCG.[26]

After conditioning with borate buffer (0.1 M sodium borate pH 9.0, 1 M NaCl), subsequent injections of running buffer were performed (startup cycles) in order to stabilize the baseline signal. The BSA was deposited on *channel 1* surface at 1 mg ml^{-1} concentration, while *channel 2* was used as the reference channel, providing the reference signal (see Fig. 1). The irreversibly deposited BSA amount was at a surface density of around 540 pg mm^{-2}. After several injections, the sample EGCG solutions were injected in different concentrations (lowest concentration: 0.533 μM, highest: 17.5 mM, dilution factor: 2, number of dilutions: 12, replicates: 2). Sample depletion was negligible in this configuration. In order to correct the measured data for the difference in how the bulk refractive index is sensed, DMSO calibration with different concentrations of DMSO solutions was additionally performed. The need of this correction originates from the fact that the reference channel does not have the ligand protein (in this case BSA) and, therefore, it is more sensitive to the changes of refractive index of the solution (also called missing volume effect in literature[48]), data adjustment and correction (DMSO calibration and DMSO-correction, baseline-correction, X (time)-offset elimination) as well as analysis of the given data were carried out using the Creoptix WAVEcontrol software.

Analysis of biosensor data. Basically, the adjusted data were evaluated with two different models. The first model supposes only one EGCG-binding site on the BSA (in the WAVEcontrol evaluation program given as 1 : 1 kinetic or hereafter homogeneous binding site model). The other one considers two binding sites with different affinities (in the WAVEcontrol evaluation program given as heterogeneous ligand or hereafter heterogeneous binding site model). Both the kinetic curves and equilibrium curves were used for the determination of K_d values. The adsorbed mass recorded at 55 min of the association section of the binding experiments was used for further analysis. Additionally, the Hill model was also used to evaluate the data in terms of the number of available binding sites on the BSA molecules:

$$R = R_{max}\frac{c^h}{K_d^h + c^h} \quad (1)$$

where R is the obtained response signal (mass) values for separate concentrations, R_{max} is the maximal response value for a given analyte concentration and c is the analyte concentration.

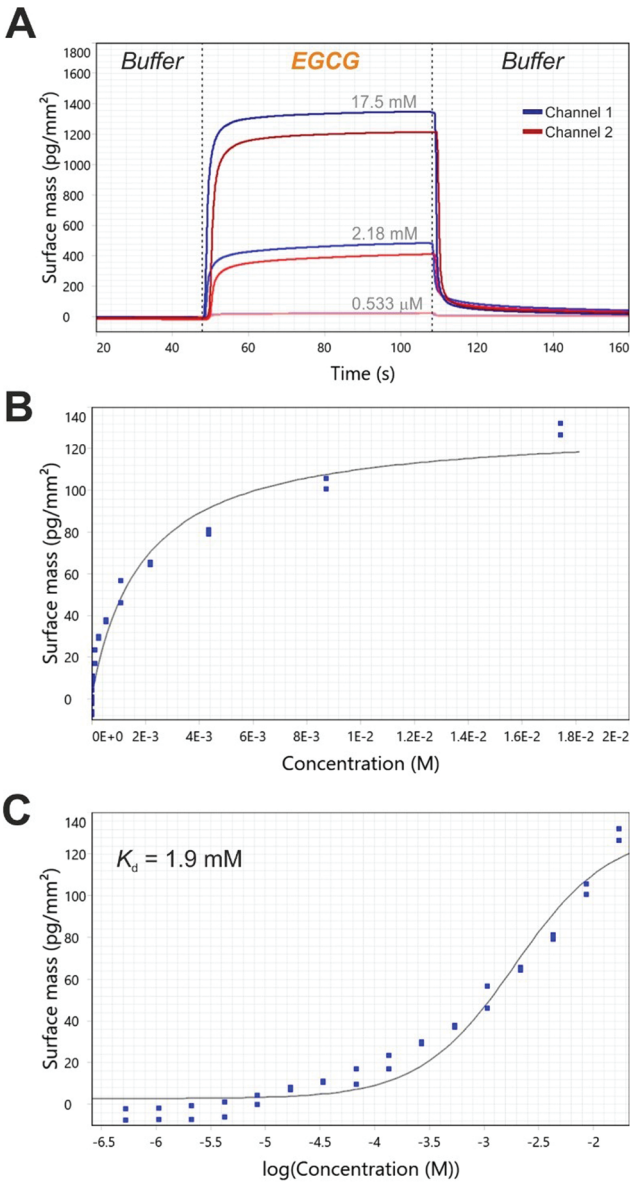

Fig. 2 Results of typical BSA–EGCG binding experiments. The measured data were evaluated using the WAVEcontrol built-in homogeneous binding site model. (A) Adsorbed surface mass values of EGCG at concentrations of 0.533 μM, 2.18 mM and 17.5 mM performed on PCP WAVEchips. Blue line: adsorption onto BSA-coated surface (*channel 1*); red line: adsorption onto reference channel surface without BSA (*channel 2*). (B) EGCG adsorption isotherm on BSA surface. (C) Surface mass – log(concentration) curve used for the determination of K_d. The data (two replicates are shown at each concentration) were fitted by the homogeneous binding site equilibrium model.

The h parameter equals to 1.0 when a monomer binds with non-cooperativity to one site. When it is greater than 1.0, the receptor or ligand has multiple binding sites with positive cooperativity. This means that the binding of a ligand makes further binding easier. h is less than 1.0 when there are multiple binding sites with different affinities for the ligand or when there is a negative cooperativity meaning that binding of a ligand inhibits the binding of further ligands.

The Hill model evaluation was performed by the GraphPad Prism 7 (demo version) software.

Results and discussion

BSA–EGCG interaction, related to literature data

Prior to the BSA–EGCG binding experiments, first the non-specific binding capabilities of various chip surfaces were tested employing EGCG solutions. We found that EGCG can bind to all of the tested surfaces at a similar level. For details, see ESI.†

Typical surface mass curves obtained on the binding of EGCG are plotted in Fig. 2A. According to our measurements on the reference channel, significant signal could be observed on surfaces without BSA coating, demonstrating the strong adsorption of EGCG even on antifouling surfaces. However, owing to the reference channel measurements, the reference-corrected differential data could be efficiently used for the kinetic and equilibrium evaluations.

As Skrt *et al*. used a single binding model to evaluate the BSA–EGCG interaction,[21] we also applied a homogeneous binding site model to fit our data in order to calculate K_d. The results of the equilibrium analysis can be seen in Fig. 2B and C. Furthermore, based on the NMR and isothermal titration calorimetry (ITC) results of Eaton *et al*.[9] who identified two binding sites with different affinity, we evaluated our data using a heterogeneous ligand model, supposing two types of differently interacting binding sites on BSA. According to our analysis based both on the kinetic and equilibrium analysis, it was found that supposing homogeneous binding sites on the EGCG, the K_d is in the 1.4–1.7 mM range. Considering binding sites with different affinities, two types of binding sites could be identified: one with K_d value of 1.7–8.6 mM and one with 0.085–0.087 mM.

To compare our results with reference K_d, the found literature K_d values of BSA-EGCG interaction are summarized in Table 1, but given as the original data found in the literature and expressed in mM. It is important to emphasize that the literature values vary in a wide range and data with several order of magnitude differences are typical. Also, the K_d values strongly depend on the applied determination method. It should be highlighted that our K_d results are closest to the NMR and ITC measurement data.[9]

BSA–ox. EGCG interaction

Typical surface mass curves obtained on the binding of ox. EGCG are plotted in Fig. 3A, and the evaluated kinetic and equilibrium results can be seen in graph **B** and **C**. In our previous study, we found that a higher amount of ox. EGCG can adsorb onto PLL-*g*-PEG and PLL-*g*-PEG-RGD surfaces compared to fresh EGCG.[26] Here, we observed a similar phenomenon, that a higher amount of ox. EGCG adsorbed on the BSA surface.

Based on the homogeneous binding site model evaluations, K_d values of 1.0–1.9 mM were determined (note, however, that the binding was overstoichiometric). Using the heterogeneous binding site model, also as for fresh EGCG, a weaker and a stronger binding sites were found (a weaker with $K_{d,1}$ = 1.8–6.5 mM and a stronger with $K_{d,2}$ = 0.039–0.13 mM). In our previous study, we found that the ox. EGCG molecules are primarily in dimer or oligomer form with higher polymerization degrees in their aqueous solutions.[26] Thus, if we consider a higher molecular weight for the analyte EGCG (*e.g.* twice or three times of the original 458 Da molecular weight) the determined K_d data using the same 458 Da molecular weight should represent apparent values. Therefore, lower actual K_d values and stronger interactions are suggested between the ox. EGCG and BSA (the obtained K_d values should be halved). Based on the above considerations and the obtained K_d data, it can be concluded that ox. EGCG molecules have higher affinity to BSA than fresh EGCG.

Our results also show that the K_d values provided by the kinetic evaluation are in the same range as the equilibrium evaluation emphasizing the potential of measuring the kinetics of interactions by the GCI technique. The measured kinetic data related to multiple concentrations as well as the fit of the data with the homogeneous and heterogeneous

Table 1 Comparison of our determined K_d values with data originating from previously published studies on BSA–EGCG interactions

Reference	Technique	Data as found in the literature	Literature data expressed in mM
Eaton, 2017[9]	Nuclear magnetic resonance (NMR)	$K_{d,1}$ = 19 μM	1.90×10^{-2} ($K_{d,1}$)
		$K_{d,2}$ = 40 mM	4.00×10^{1} ($K_{d,2}$)
Eaton, 2017[9]	Isothermal titration calorimetry (ITC)	$K_{d,1}$ = 21.6 μM	2.16×10^{-2} ($K_{d,1}$)
		$K_{d,2}$ = 22 mM	2.20×10^{1} ($K_{d,2}$)
Zinellu, 2014[49]	Affinity capillary electrophoresis (ACE)	$K_b = 3.68 \times 10^4$ M^{-1}	2.72×10^{-2}
Chandra, 2012[50]	Fluorescence quenching	$K_b = 4.00 \times 10^5$ M^{-1}	2.50×10^{-3}
Skrt, 2012[21]	Fluorescent emission spectrometry	$K_b = 14.0 \times 10^5$ M^{-1}	2.17×10^{-3}
Zhang, 2016[10]	Docking analysis	ΔG = −10 kcal mol^{-1}	4.68×10^{-8}

Data indications are the followings: K_d: dissociation constant ($K_{d,1}$ or $K_{d,2}$ refers to the dissociation constants of two separate binding sites), K_b: binding constant (reciprocal to K_d), ΔG: Gibbs free energy change accompanying the binding event.

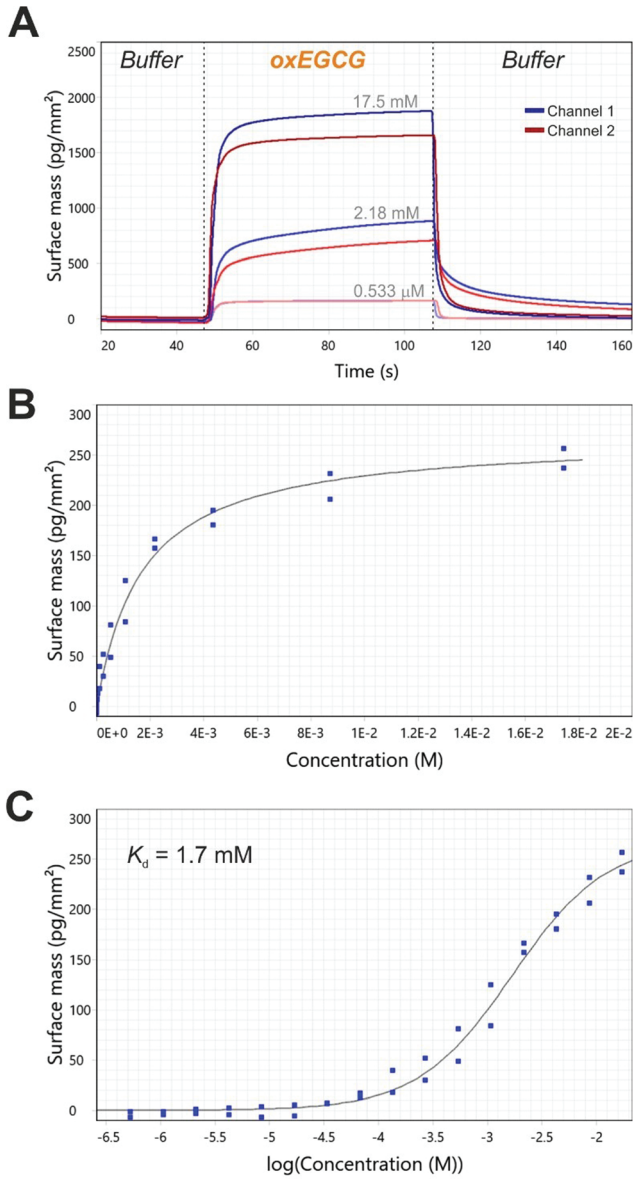

Fig. 3 Results of typical BSA–ox. EGCG binding experiments performed on PCP WAVEchips. The measured data were evaluated using the WAVEControl built-in homogeneous binding site model. (A) Adsorbed surface mass values of ox. EGCG at concentrations of 0.533 μM, 2.18 mM and 17.5 mM. Blue line: adsorption onto BSA-coated surface (*channel 1*); red line: adsorption onto reference channel surface without BSA (*channel 2*). (B) ox. EGCG adsorption isotherm on BSA surface. (C) Surface mass – log(concentration) curve used for the determination of K_d. The data (two replicates are shown at each concentration) were fitted by the homogeneous binding site equilibrium model.

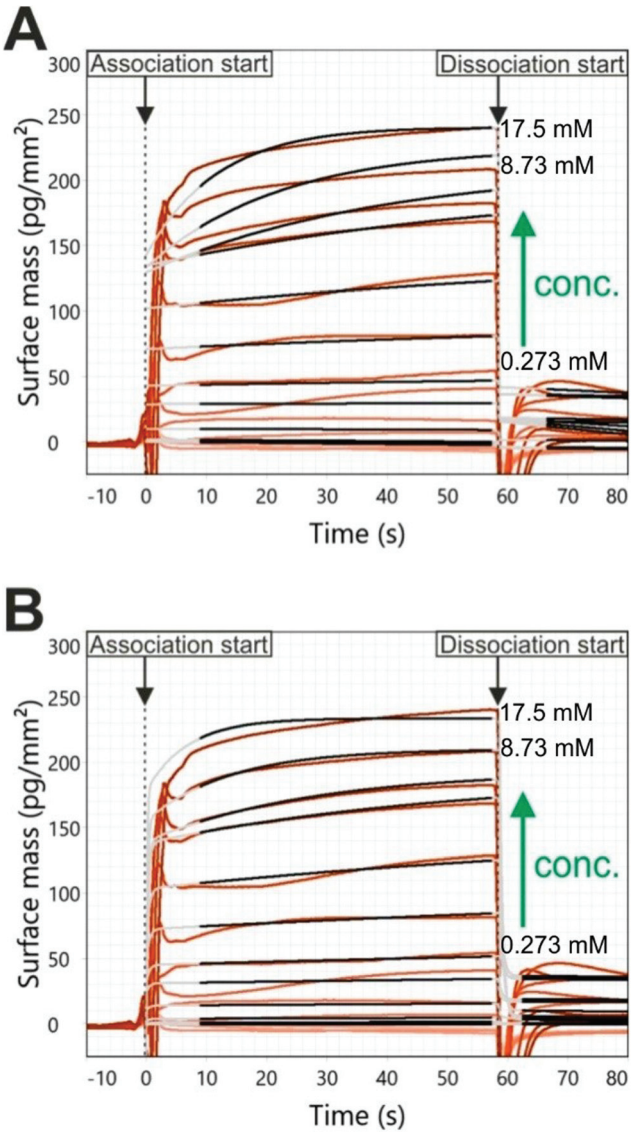

Fig. 4 Fitting the adjusted and reference-corrected data with the homogenous (A) and heterogeneous (B) kinetic models in case of ox. EGCG. The individual red curves represent separate association and dissociation phases obtained at different ox. EGCG concentrations. The green arrow indicates the direction of concentration increase: the top curve corresponds to the highest ox. EGCG concentration (17.5 mM), while the curves underneath correspond to lower concentrations following a decreasing concentration order: 17.5 mM, 8.73 mM, 4.36 mM, 2.18 mM, 1.09 mM, 0.546 mM, 0.273 mM, 0.136 mM, 68.2 μM, 34.1 μM, 17.1 μM, 8.52 μM, 4.26 μM, 2.131 μM, 1.07 μM, 0.533 μM. Only the 17.5 mM, 8.73 mM as well as 0.273 mM concentrations are marked at the maximal signal value. Replicated measurements are not shown. χ^2 error function values representing the quality of fit: homogeneous model (lower value represents a better fit): 7.5 pg mm^{-2}, heterogeneous model: 5.8 pg mm^{-2}.

binding site kinetic models are shown in Fig. 4. According to the fit evaluations, the quality of the fit was better in case of the heterogeneous model (see χ^2 error function values of fits in figure caption).

Consideration of multiple binding sites, Hill model evaluation

Comparing the measured maximal response value (R_{max}) with an expected response that corresponds to the case when one BSA molecule binds one EGCG or ox. EGCG, we calculated the number of EGCG and ox. EGCG molecules bound by one BSA molecule. The number of bound EGCG and ox. EGCG/BSA can be seen in Table 2. Additionally, the K_d values resulted from the evaluations are also included in the table. It is important

Table 2 Summary of data obtained on the binding of EGCG and ox. EGCG to BSA. Note that in case of ox. EGCG, EGCG molecules are mostly in dimerized form (the shown apparent K_d values of ox. EGCG should be halved)

			Homogenous binding site model		Heterogeneous binding sites model				
					Kinetic Fit		Equilibrium		
	Measured R_{max} (pg mm^{-2})	Bound EGCG/BSA	Kinetic fit K_d (mM)	Equilibrium K_d (mM)	$K_{d,1}$ (mM)	$K_{d,2}$ (mM)	$K_{d,1}$ (mM)	$K_{d,2}$ (mM)	Hill coeff.
EGCG	134	35	1.4	2.0	1.7	0.085	8.6	0.087	0.50
ox. EGCG	240	63	1.0	1.6	6.5	0.13	1.8	0.039	0.91

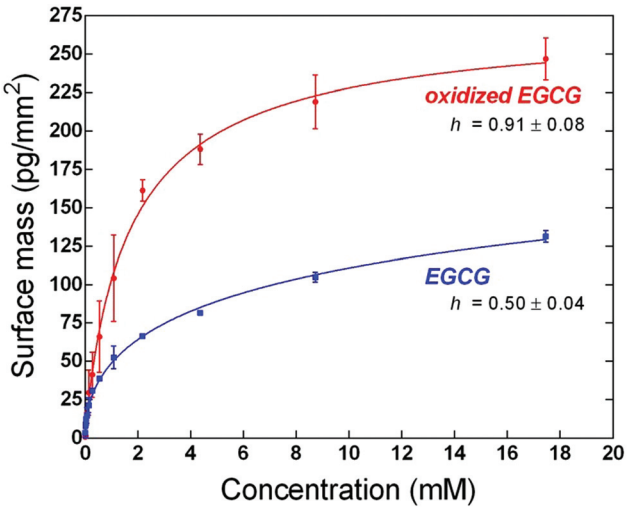

Fig. 5 Fitting of EGCG and ox. EGCG data points with the Hill model. The obtained Hill coefficient values (h) are less than 1.0 indicating multiple binding sites.

to note that considering the deposited BSA amount and subsequently bound EGCG one can safely suggest that there are multiple binding sites on each BSA molecule for EGCG (35 and 63 EGCG and ox. EGCG molecules/BSA, respectively). Thus, the Hill model that fits the Hill coefficient (also known as Hill slope, h) was also used for the evaluation.

As a result of Hill equation fits, we obtained Hill coefficient values less than 1.0 both for EGCG (h = 0.50 ± 0.04) and ox. EGCG (h = 0.91 ± 0.08). Based on these outcomes, we suggest that there are multiple binding sites on the BSA. After the stronger binding site saturates, other EGCG molecules bind to weaker sites, which means that the binding of an EGCG ligand inhibits the binding of further EGCG molecules. The fitted curve is plotted in Fig. 5.

Conclusions

In this work, we have presented a quantitative characterization on the interaction of the polyphenol EGCG and its poorly studied oxidized form (ox. EGCG) with BSA protein using a highly sensitive label-free optical biosensor (GCI). This technique enables to collect reference-corrected kinetic data about molecular binding events. As the data obtained on the reference channel revealed, EGCG (and also ox. EGCG) adsorbs to all types of chip surfaces at around the same level, independently on the hydrophilicity/hydrophobicity of the chip surfaces. This is an important information for those who are studying this molecule. The comparison of the measured and expected R_{max} values revealed that BSA has several binding sites for capturing EGCG, the binding is overstoichiometric. According to our results, one BSA molecule is able to bind up to 35 EGCG or 63 ox. EGCG molecule, respectively. Using the Hill model for evaluating the equilibrium data, the obtained h parameters confirmed that there are multiple binding sites ($h < 1$). The binding of the first EGCG molecule has an inhibition effect on further EGCG binding. Based on the kinetic and equilibrium analysis, in case of using a homogeneous binding site model, the K_d values characterizing the EGCG/ox. EGCG–BSA interaction were in the mM range. The applied heterogeneous binding site model revealed that BSA has stronger and weaker binding sites, which could be characterized by two separate K_d values (one in the mM range and one in the 10^{-2}–10^{-1} mM range, respectively). Our data have shown that more ox. EGCG bound to the BSA than fresh EGCG. This observation is similar to the behavior of EGCG/ox. EGCG on PLL-*g*-PEG coatings.[26] It can be concluded that without using reference-correction, the above phenomena could not be revealed. The presented method could be extended to various types of analytes and ligands, also using various reference surfaces with wide range of surface chemistries. The above results also highlight the importance of polyphenol oxidization in conjunction with their transport properties in the body.

Conflicts of interest

There are no conflicts to declare.

Acknowledgements

This work was supported by the Momentum Program ("Lendület") of the Hungarian Academy of Sciences and by the ERC_HU, KH_17 and KKP_19 programs of NKFIH. The continuous support of Creoptix AG, especially the discussions with Kaspar Cottier and Fabio Spiga, is gratefully acknowledged.

References

1 B. Peter, S. Bosze and R. Horvath, *Eur. Biophys. J.*, 2017, **46**, 1–24.
2 B. N. Singh, S. Shankar and R. K. Srivastava, *Biochem. Pharmacol.*, 2011, **82**, 1807–1821.
3 H. Mukhtar and N. Ahmad, *Am. J. Clin. Nutr.*, 2000, **71**, 1698–1702.
4 J. Hong, H. Lu, X. Meng, H.-H. Colon, J. Ryu, Y. Hara and C. S. Yang, *Cancer Res.*, 2002, **62**, 7241–7246.
5 H. Tachibana, *Proc. Jpn. Acad., Ser. B*, 2011, **87**, 66–80.
6 S. Hirun and P. D. Roach, *Int. Food Res. J.*, 2011, **18**, 1261–1264.
7 Z. Hou, S. Sang, H. You, M. J. Lee, J. Hong, K. V. Chin and C. S. Yang, *Cancer Res.*, 2005, **65**, 8049–8056.
8 M. Li and A. E. Hagerman, *J. Agric. Food Chem.*, 2014, **62**, 3768–3775.
9 J. D. Eaton and M. P. Williamson, *Biosci. Rep.*, 2017, **37**, BSR20170209.
10 Y. Zhang, Y. Y. Xu, W. J. Sun, M. H. Zhang, Y. F. Zheng, H. M. Shen, J. Yang and X. Q. Zhu, *Biomed Res. Int.*, 2016, **2016**, 1–8.
11 C. S. Yang, H. Wang, J. X. Chen and J. Zhang, *Effects of Tea Catechins on Cancer Signaling Pathways*, Elsevier Inc., 1st edn, 2014, vol. 36.
12 H. S. Davies, P. D. A. Pudney, P. Georgiades, T. A. Waigh, N. W. Hodson, C. E. Ridley, E. W. Blanch and D. J. Thornton, *PLoS One*, 2014, **9**, e108372.
13 P. Georgiades, P. D. A. Pudney, S. Rogers, D. J. Thornton and T. A. Waigh, *PLoS One*, 2014, **9**, e105302.
14 S. A. Hudson, H. Ecroyd, F. C. Dehle, I. F. Musgrave and J. A. Carver, *J. Mol. Biol.*, 2009, **392**, 689–700.
15 S. A. Mandel, T. Amit, O. Weinreb, L. Reznichenko and M. B. H. Youdim, *CNS Neurosci. Ther.*, 2008, **14**, 352–365.
16 Y. Fujimura, M. Sumida, K. Sugihara, S. Tsukamoto, K. Yamada and H. Tachibana, *PLoS One*, 2012, **7**, e37942.
17 E. H. Byun, T. Omura, K. Yamada and H. Tachibana, *FEBS Lett.*, 2011, **585**, 814–820.
18 Z. Li, J. Ha, T. Zou and L. Gu, *Food Funct.*, 2014, **5**, 1278.
19 A. Nozaki, M. Hori, T. Kimura, H. Ito and T. Hatano, *Chem. Pharm. Bull.*, 2009, **57**, 224–228.
20 M. Kusuda, T. Hatano and T. Yoshida, *Biosci. Biotechnol. Biochem.*, 2006, **70**, 152–160.
21 M. Skrt, E. Benedik, Č. Podlipnik and N. P. Ulrih, *Food Chem.*, 2012, **135**, 2418–2424.
22 X. Wang, C.-T. Ho and Q. Huang, *J. Agric. Food Chem.*, 2007, **55**, 4987–4992.
23 Q. Y. Zhu, A. Zhang, D. Tsang, Y. Huang and Z. Y. Chen, *J. Agric. Food Chem.*, 1997, **45**, 4624–4628.
24 K. J. Siebert, N. V. Troukhanova and P. Y. Lynn, *J. Agric. Food Chem.*, 1996, **44**, 80–85.
25 F. Höök, B. Kasemo, T. Nylander, C. Fant, K. Sott and H. Elwing, *Anal. Chem.*, 2001, **73**, 5796–5804.
26 B. Peter, E. Farkas, E. Forgacs, A. Saftics, B. Kovacs, S. Kurunczi, I. Szekacs, A. Csampai, S. Bosze and R. Horvath, *Sci. Rep.*, 2017, **7**, 42220.
27 J. Vörös, J. Ramsden, G. Csúcs, I. Szendrő, S. De Paul, M. Textor and N. Spencer, *Biomaterials*, 2002, **23**, 3699–3710.
28 E. Migliorini, M. Weidenhaupt and C. Picart, *Biointerphases*, 2018, **13**, 06D303.
29 M. C. Estevez, M. A. Otte, B. Sepulveda and L. M. Lechuga, *Anal. Chim. Acta*, 2014, **806**, 55–73.
30 R. Gupta and N. J. Goddard, *Analyst*, 2013, **138**, 3209–3215.
31 R. Gupta and N. J. Goddard, *Analyst*, 2013, **138**, 1803–1811.
32 D. Kotlarek, M. Vorobii, W. Ogieglo, W. Knoll, C. Rodriguez-Emmenegger and J. Dostálek, *ACS Sens.*, 2019, **4**, 2109–2116.
33 U. Hohmann, J. Nicolet, A. Moretti, L. A. Hothorn and M. Hothorn, *Nat. Plants*, 2018, **4**, 345–351.
34 B. Peter, R. Ungai-Salanki, B. Szabó, A. G. Nagy, I. Szekacs, S. Bősze and R. Horvath, *ACS Omega*, 2019, **4**, 10474–10474.
35 B. Peter, R. Ungai-Salanki, B. Szabó, A. G. Nagy, I. Szekacs, S. Bösze and R. Horvath, *ACS Omega*, 2018, **3**, 3882–3891.
36 J. McColl, R. Horvath, A. Aref, L. Larcombe, I. Chianella, S. Morgan, G. E. Yakubov and J. J. Ramsden, *J. Biomater. Sci., Polym. Ed.*, 2009, **20**, 841–851.
37 J. McColl, R. Horvath, G. E. Yakubov and J. J. Ramsden, *Int. J. Biol. Macromol.*, 2017, **95**, 704–712.
38 D. Patko, Z. Mártonfalvi, B. Kovacs, F. Vonderviszt, M. Kellermayer and R. Horvath, *Sens. Actuators, B*, 2014, **196**, 352–356.
39 P. Kozma, A. Hámori, S. Kurunczi, K. Cottier and R. Horvath, *Sens. Actuators, B*, 2011, **155**, 446–450.
40 D. Patko, B. Gyorgy, A. Nemeth, K. E. Szabó-Taylor, A. Kittel, E. I. Buzas and R. Horvath, *Sens. Actuators, B*, 2013, **188**, 697–701.
41 D. Patko, K. Cottier, A. Hamori and R. Horvath, *Opt. Express*, 2012, **20**, 23162–23173.
42 P. Kozma, A. Hamori, K. Cottier, S. Kurunczi and R. Horvath, *Appl. Phys. B: Lasers Opt.*, 2009, **97**, 5–8.
43 B. Sepúlveda, J. S. del Río, M. Moreno, F. J. Blanco, K. Mayora, C. Domínguez and L. M. Lechuga, *J. Opt. A: Pure Appl. Opt.*, 2006, **8**, S561–S566.
44 M. C. Estevez, M. Alvarez and L. M. Lechuga, *Laser Photonics Rev.*, 2012, **6**, 463–487.
45 S. Herranz, A. F. Gavela and L. M. Lechuga, in *Methods in Molecular Biology*, ed. A. Rasooly and B. Prickril, Springer New York, New York, NY, 2017, vol. 1571, pp. 161–185.
46 J. Escorihuela, M. Á. González-Martínez, J. L. López-Paz, R. Puchades, Á. Maquieira and D. Gimenez-Romero, *Chem. Rev.*, 2015, **115**, 265–294.
47 Creoptix WAVE Brochure, https://www.creoptix.com/images/pdf/CreoptixWAVE_Brochure.pdf.
48 SPR Pages – Artefacts, https://www.sprpages.nl/best-results/artifacts?highlight=WyJtaXNzaW5nIiwibWlzcyIsInZvbHVtZSIsInZvbHVtZXMiXQ==.
49 A. Zinellu, S. Sotgia, B. Scanu, E. Pisanu, R. Giordo, A. Cossu, A. M. Posadino, C. Carru and G. Pintus, *J. Chromatogr. A*, 2014, **1367**, 167–171.
50 G. K. Chandra, D. R. Tripathy, A. Roy and S. Dasgupta, *Appl. Spectrosc.*, 2012, **66**, 75–81.

